

# INTEGRATED ACOUSTO OPTICAL TUNABLE FILTERS (AOTFs): DEVELOPMENT, TECHNOLOGY AND APPLICATIONS

PACS REFERENCE: 42.79.J

Varasi M. <sup>(1)</sup>; Verona E. <sup>(2)</sup>

<sup>(1)</sup> Alenia Marconi Systems, Via Tiburtina Km 12.400, I-00131 Roma, Italy.  
Tel: +39 06 4150 2315, Fax: +39 06 4150 3701, e-mail: [mvarasi@amsjv.it](mailto:mvarasi@amsjv.it)

<sup>(2)</sup> CNR-Ist. di Acustica "O.M. Corbino", Via del Fosso del Cavaliere, 100, I-00133 Roma, Italy.  
Tel: +39 06 4993 4481, Fax: +39 06 2066 0061, e-mail: [verona@idac.rm.cnr.it](mailto:verona@idac.rm.cnr.it)

## ABSTRACT

The design of integrated optical AOTFs, together with the technologies required for their fabrication, have been developed for applications in the fields of Wavelength Division Multiplexing (WDM) in Optical Fiber Communication systems (OFC), optical processing and distribution of microwave signals, and, finally, to realise portable instrumentation for Fibre Bragg Grating (FBG) sensors signal processing. The technology is described and particular achievements are discussed in order to improve the resolution and sidelobe ratio. The AOTF is a key device in the development of WDM-OFC systems, in which it carries add-drop functions as well as active filtering. The wavelength filtering function is also used in those optical beam forming networks for active array radar antennas, in which the optical domain is exploited to process and distribute the microwave signals. The AOTF based instrumentation makes possible the full exploitation of the FBG sensor systems in harsh environments.

## INTRODUCTION

The evolution of OFC systems towards WDM architectures requests for active filters with high performances in terms of resolution, Signal to Noise ratio (S/N), speed and losses. The integration of the AOTF concept in a planar optical circuit in LiNbO<sub>3</sub> offers a flexible solution to the many requested functionalities. The potentially huge dimension of the OFC market drives the technological evolution of this family of devices, and other nice application fields are exploiting this opportunity. The architecture for microwave signal processing in defence systems and the processing of optical signal for Fiber Bragg Grating sensor systems are two relevant examples of that. The increasing use of FBG sensors in structural monitoring induces the request of fibre compatible, portable, rugged and low cost instrumentation for the processing of the optical signals from FBG sensors to monitor local static and dynamic stresses and strains. In this unconventional application the AOTF is the core device, the filter, of very rugged and compact instrumentation realised in integrated optical configuration.

## ACOUSTO OPTIC TUNABLE FILTER

The Acousto Optical Tunable Filter [2] is implemented on a x-cut LiNbO<sub>3</sub> substrate, according to the scheme shown in Fig. 1. It consists of two elementary AOTFs, operating in parallel, in order to process both the polarisations of the optical input. The design and the fabrication processes of the device are optimised in order to improve the optical wavelength resolution, the sidelobe ratio and to make the device operation not sensitive to the optical polarisation, as required by the different applications.

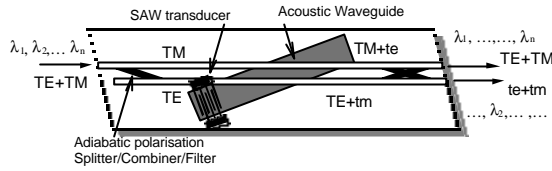


Fig. 1. Schematic view of the generic AOTF optical circuit

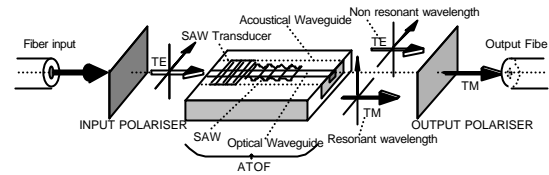


Fig. 2. Schematic view of the components integrated in the AOTF planar circuit

The elementary AOTF circuit exploits a collinear acoustooptic interaction between the guided optical radiation and the surface acoustic wave, both propagating along the y- axis of the LiNbO<sub>3</sub> substrate. The interaction gives rise to the transfer of optical power between the two polarizations of the guided optical radiation, when the following phase matching relationships are satisfied:

$$\vec{K}_{TE} + \vec{K}_A = \vec{K}_{TM} \quad \vec{K}_{TM} - \vec{K}_A = \vec{K}_{TE} \quad (1)$$

being Eq. 1 the vectorial description (momentum conservation) of the collision between the input photon  $\vec{K}_{TE}$  or  $\vec{K}_{TM}$  and phonon  $\vec{K}_A$  to produce the output photon  $\vec{K}_{TM}$  or  $\vec{K}_{TE}$ . Because of the collinear nature of the collision, from the scalar version of Eq. 1 we have:

$$\lambda_p = v(n_{TM} - n_{TE}) / f \quad (2)$$

where  $\lambda_p$  is the optical wavelength, at the peak of the interaction,  $v$  and  $f$  are the phase velocity and the frequency of the SAW, and  $n_{TM}$ ,  $n_{TE}$  the effective refractive indexes of the guided optical polarizations TM and TE, respectively. When the elementary AOTF is interposed between two crossed polarisers, as shown in Fig. 2, the optical transmission function of the system is the Fourier transform of the acoustic energy distribution along the interaction length. For a constant amplitude of the acoustic wave, the transfer function is a sinc<sup>2</sup> function, centred at  $\lambda_p$ . The device acts as an optical filter, tuneable by the acoustic frequency and with a FWHM given by:

$$\Delta\lambda_p = 0.8\lambda_p^2 / L\Delta n \quad (3)$$

being  $L$  the length of the acoustooptic interaction region and  $\Delta n = n_{TM} - n_{TE}$ .

### Fabrication of the AOTF

The optical circuit (see Fig. 1) includes two interaction regions between two polarisation splitter/combiners. In the solution here proposed, this key device, the polarisation splitter/combiner, is realised by an adiabatic coupling between the titanium indiffused optical waveguide and a Thermal Annealed Proton Exchange (TAPE) waveguide. This solution allows to avoid the thermal instabilities of polarisation splitters based on the interference between modes.

### High Sidelobe Ratio: AO Interaction Apodisation by Thin Film Acoustic Waveguides

The fabrication of the Surface Acoustic Wave (SAW) channel waveguide requires a local change of the acoustic propagation velocity of the substrate, shaped according to the desired guiding structure. The change in the velocity can be obtained either by the modification of the surface elastic properties of the substrate, or by deposition of a thin film of a suitable material: the acoustic energy will be confined in the region where the velocity is lower. Among the different possible techniques, such as deep Ti indiffusion in the cladding regions, low phase-velocity film deposition in the core regions or high phase-velocity film deposition in the cladding region, we have chosen the last because of several advantages: it doesn't perturb the SAW propagation, and the technology is quite simpler. Finally a few materials, such as Al<sub>2</sub>O<sub>3</sub>, AlN and MgO, showing a fairly high-phase velocity are available, that can be easily deposited in the form of thin films, using

conventional sputtering techniques. Fig. 3 shows the phase velocity dispersion curves, together with the relative change in the phase velocity for a yx-LiNbO<sub>3</sub> substrate covered with a zx-oriented film of AlN, Al<sub>2</sub>O<sub>3</sub> and MgO.

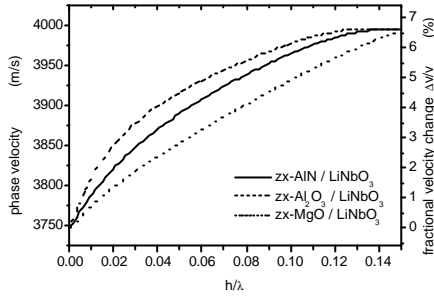


Fig. 3. Phase velocity dispersion curves and relative changes in the phase velocity for zx-oriented films of AlN, Al<sub>2</sub>O<sub>3</sub> and MgO on yx-LiNbO<sub>3</sub>.

The acoustic waveguide supports a discrete set of guided modes, whose propagation velocity  $v$  depends on the physical and geometrical parameters, according to the dispersion relation [4]:

$$\frac{1}{2}aK_{ys} = m \frac{\pi}{2} + \tan^{-1} \left( \frac{K_{yf}}{K_{ys}} \right) \quad \text{with} \quad K_{ys} = \sqrt{\left( \frac{\omega}{v_s} \right)^2 - \left( \frac{\omega}{v} \right)^2} \quad K_{yf} = \sqrt{\left( \frac{\omega}{v} \right)^2 - \left( \frac{\omega}{v_f} \right)^2} \quad (4)$$

being  $a$  the width of the guide,  $\omega$  the angular frequency of the acoustic wave ( $\omega=2\pi f$ ),  $m$  an integer, corresponding to the order of the guided mode, and  $v$  and  $v_s$  the SAW phase velocities in the cladding and in the substrate regions, respectively.

By exploiting acoustic waveguides showing a variable width and/or the acoustic coupling between waveguides, it is possible to modulate the SAW amplitude along the interaction region (apodisation) in order to increase the sidelobe ratio of the acoustooptic transmission function.

#### High Resolution

The request for narrow-band AOTF transmission function is common to the many applications, and is one of the most critical in terms of technological constrains. Equation 3 suggests that the increase in the interaction length is the the only way to iprove the filter resolution. The use of 4" wafers allows to realise interaction lengths up to 78 cm. In these conditions the maximum fabrication process uniformity is mandatory, in order to ensure the necessary uniformity to the acousto-optic coupling conditions along the interaction region [5] .

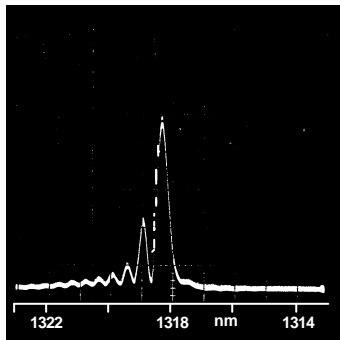


Fig. 4. Experimental AOTF transmission function with evidence of degraded sidelobe ratio.

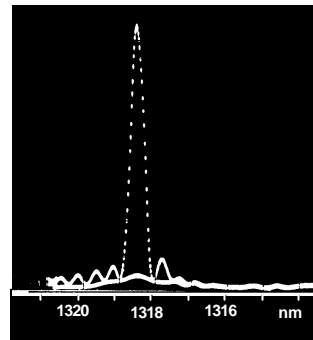


Fig. 5. Experimental transmission function of AOTF including the compensation of the  $\Delta n$  inhomogeinity

Residual process disuniformities cause an asymmetric sidelobe degradation in the filter transmission function. An experimental result is shown in Fig. 4 as obtained using an high uniformity standard processed high resolution AOTF ( $L=4$  cm) and SAW waveguide parallel to the optical waveguides. The asymmetry in the sidelobes and the  $-4.5$  dB sidelobe ratio have to be compared with the symmetrical sidelobes distribution and the  $-9.6$  dB sidelobe ratio expected in a  $\text{sinc}^2$  condition. In order to analyse the problem, a simplified mathematical model has been adopted for the collinear acousto-optical interaction, where the evolution of the complex optical mode field amplitudes  $E_{TE}$  and  $E_{TM}$  are given by the solution of the following coupled mode equations system:

$$\frac{dE_{TE}}{dy} = kE_{TM} \exp\{-iy\beta\} \quad (5.1) ; \quad \frac{dE_{TM}}{dy} = -kE_{TE} \exp\{iy\beta\} \quad (5.2)$$

where  $k$  is the coupling coefficient between the two modes,  $y$  is the spatial coordinate along the interaction region, and  $\beta = \Delta n/\lambda - f/v$  is the phase matching parameter.

By using this model it is possible to correlate the observed asymmetry with a parabolic variation of the parameter  $\Delta n$  along the  $y$  direction, centered at  $L/2$ , as expressed by:

$$\Delta n(y) = \Delta n_0 \left\{ 1 - \alpha \left[ 1 - \frac{2y}{L} \right]^2 \right\} \quad (6)$$

Where  $\Delta n_0$  is the unperturbed difference between the effective refractive indexes of the TE and TM guided modes, and  $\alpha$  is the parabolic perturbation coefficient. By including this perturbation in the model, it is possible to obtain simulations in matching the experimental results. It is then possible to find a solution, at design level, able to compensate this effect. That is possible simply observing that a dependence of the acoustic velocity on the spatial coordinate  $y$  can compensate the variation of the effective refractive index difference  $\Delta n(y)$  in the expression of  $\beta$ .

$$v(y) = v \left\{ 1 - \xi \left[ 1 - \frac{2y}{L} \right]^2 \right\} \quad (7)$$

If a dependence in the SAW velocity is introduced as shown in Eq. 7, a  $\beta$  constant along the interaction length can be obtained, provided  $\xi$  satisfies the following expression:

$$\xi = - \left( \frac{\Delta n_0 v}{f\lambda} \right) \alpha \quad (8)$$

The spatial dependence of the SAW velocity has been introduced by using an acoustic waveguide whose width follows a parabolic function of the  $y$  coordinate, centered at  $L/2$ , and able to satisfy the conditions of Eq. 8. This solution allowed us to solve the problem, and the repeatability of the results was validated by a significant number of production runs. A typical experimental result is shown in Fig. 5, where the FWHM is 0.43 and the sidelobe ratio is lower than 9 dB, in good agreement with the expected value working in the 1300 nm wavelength range.

## AOTF FOR WDM OFC SYSTEMS

WDM and Dense WDM (DWDM) systems, request for advanced solutions to process optical signals in present and future architectures. The AOTF is the key to give the solution to the add/drop multiplexing, the optical amplifier gain flattening and other critical issues of these architectures. Higher speed, remote reconfigurability and flexibility to a wide range of requirements are among the advantages offer by AOTF over the other solutions as FBG in the processing of the multi-wavelength signal.

## AOTF FOR OPTICAL PROCESSING OF MICROWAVE SIGNALS

The evolution of the antenna systems towards multifunctionality in radar sensors, Electronic Counter Measurements (ECM), Electronic Surveillance Measurement (ESM) and Communication induces the request for new technological approaches to face the wide instantaneous/operating bandwidth, high dynamic range and electromagnetic compatibility requirements. The optical processing of the microwave signal offers a wide range of solutions which give significant advantages in comparison with the all electronic processing of the signals.

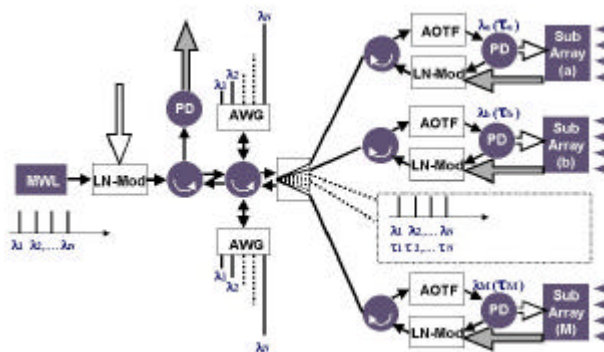


Fig. 6. Example of architecture for TxRx distribution of signals in Phased Array Active Antennas

The AOTF is the key device in an Optical Beam Forming Network (Fig. 6) where the True Time Delay (TTD) function is achieved by different fiber lengths experimented by the wavelengths in a WDM architecture. The AOTF is used to select the wavelength and then the delay to be addressed to each sub-arrays. This TxRx architecture is particular attractive for those applications, like ESM and ECM, in which the bandwidth a very wide (2-18 GHz).

### AOTF BASED INSTRUMENTATION FOR FBG SENSOR SYSTEMS

The FBG sensor is a grating realised by UV holography in an optical monomode fibre [1], and reflects radiation which wavelength satisfies the Bragg relation:  $\lambda_B = 2n\Lambda$ , being  $n$  the effective refractive index of the fibre and  $\Lambda$  the period of the grating. The fibre follows the stress status of the structure in which it is embedded or onto which is attached, and compressive or tensile stresses parallel to the fibre axis at the location of the FBG induce changes in  $\lambda_B$  in accordance with the relation (9):

$$\Delta\lambda_B / \lambda_B \approx (1 - p_e)\varepsilon \quad (9)$$

where  $p_e$  is the effective photoelastic constant of the fibre and  $\varepsilon$  is the deformation measured in  $\mu$ strains. The conventional instrumentation interfaced to FBG sensors, based on Optical Spectrum Analysers, dramatically limits the industrial application of the system mainly because of its weight, volume, sensitivity to vibrations and low scanning speed.

The AOTF, driven by a Voltage Controlled Oscillator (VCO) which allows to control the tuning of the filter by a simple DC voltage, is the key element of a very effective instrumentation, enabling three main operating modes [3]: spectrometer, discriminator and tracking filter.

The spectrometer configuration is the simplest operating mode in which the AOTF is used as a scanning filter (Fig. 7). This operating mode is useful for measuring the static strains applied to the FBG with a sensitivity of 400  $\mu$ strains, limited by the resolution of the AOTF .

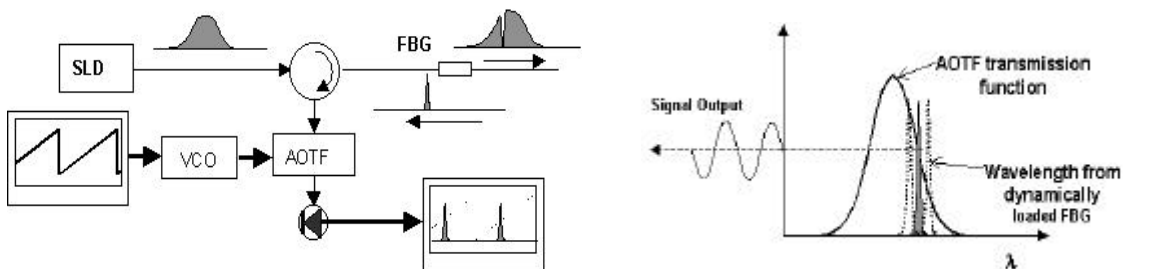


Fig. 7. AOTF instrumentation: scanning filter. Fig.8. AOTF instrumentation: discriminator.

In the discriminator configuration the opto-acoustic filter is tuned such that the sensor signal is generally positioned on the linear portion of the slope of the AOTF transmission function. The opto-acoustic filter is temporarily held in this position, and dynamic changes imposed on the fibre grating sensors can be decoded (Fig. 8). In this way dynamic strains with very high frequency content can be measured with a very high sensitivity (<10  $\mu$ strains).

In some applications the measurement of both static and dynamic strains is required and in such a case a third mode of operation may be beneficial. In the Tracking Filter operating mode the opto-acoustic filter is automatically tuned to be centered on the sensor signal of interest, even while the sensor is caused to shift from a large static perturbation (Fig. 9). This configuration allows to monitor high speed perturbation as well as large static or quasi-static load variations. Experimental results indicate a sensitivity of this instrumentation in the range of 0.1  $\mu$ strains for static deformations and 0.0023  $\mu$ strains/Hz<sup>1/2</sup> for dynamic strains. The simple spectrometer operating mode of the AOTF based instrumentation is compared to conventional Optical Spectrum Analyser in Tab. I. In spite of the reduced resolution, which can be improved by using the

discriminator or the tracking filter configuration, the highest scanning speed and the reduced size make the AOTF based instrumentation very attractive for many practical uses.

Tab. I. Comparison between AOTF (scanning filter) based instrumentation and conventional Optical Spectrum Analyser (OSA)

	Resolution ( $\delta\lambda$ ) (nm)	Range ( $\Delta\lambda$ ) (nm)	Scanning Speed (mm/s)	Optical Insertion Loss (dB)	Volume (l)
AOTF	0.4 (0.001)	300 - 600	35000	6	0.5
OSA	0.1	500	0.5	6 - 10	30

## FIELD TRIALS

The AOTF based instrumentation has been tested in many different configurations and test conditions. A simple scanning filter configuration (Fig. 10) has been used to realise an instrumentation for FBG sensors systems attached on the surface of metallic structures of a Jetstream aircraft. The system exploits wavelength as well as space division multiplexing to interrogate a large number of sensors. The light from a broadband (SLD) source is simultaneously addressed to eight identical sensorised fibres after passing through the AOTF. The FBG sensors are defined in different positions along each fibre with a distinct peak reflection wavelength at zero-strain. Each sensor is then uniquely identified in the fibre by its reflection wavelength.

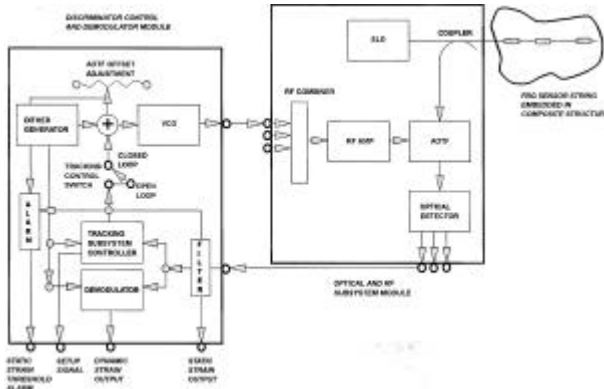


Fig. 9. Schematic layout of the three parallel channel tracking filter based instrumentation.

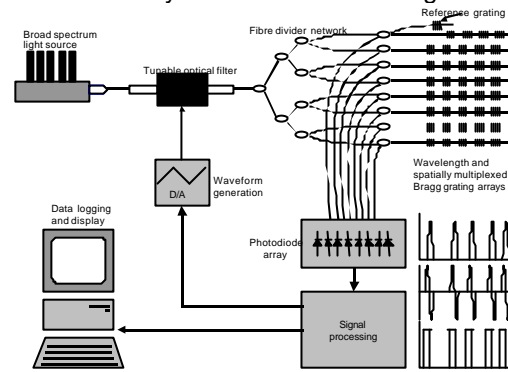


Fig. 10. Schematic diagram of the AOTF scanning filter based instrument configuration and sensor system.

The instrumentation has been used for flight tests in which the sensors were attached on the surface of the metallic structures of Jetstream 31 aircraft. Although still a prototype, the system underwent full installation and flight clearance processes and functioned without degradation during a series of 8 test flights of the flying test bed. The test flights involved rapid climbs, descents; high angle turns and repeated roller landings.



Fig. 11. Aircraft used for flight tests

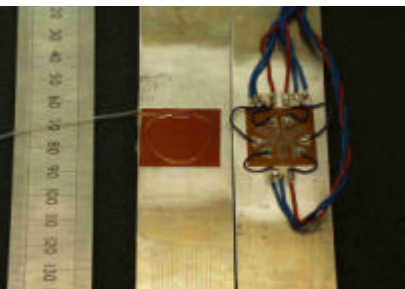


Fig.12. FBG sensors compared with electrical strain gauge

This exposed the optical fibre sensor components to rapid temperature excursions between +6 and -23°C; rapid load transitions associated with repeated take-off and landing and turning manoeuvres up to approximately 2g. The cabin-mounted, optical sensor instrumentation endured significant vibration levels typical of the mid cabin location between the twin turboprops of the Jetstream together with the g-forces and accelerations from flight manoeuvres.

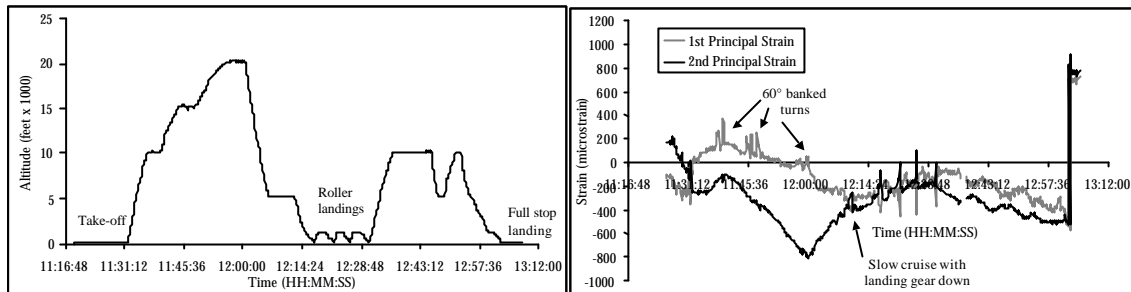


Fig. 13. Data captured during flight test .

Sensor patches were bonded to the external surface of the wing and protected with a layer of standard aerospace sealant. Three sensors were included in each patch in an optical equivalent of a 'delta' electrical strain gauge rosette, to duplicate the function of a three axis, 3 x 120° strain measurement gauge using a single optical fibre loop. A fourth sensing element, isolated from strain, was also included to measure the local temperature. An example of the optical strain gauge rosette with the equivalent electrical device for comparison is shown in Fig. 12. Typical data recorded during a flight test are shown in Fig. 13. The top graph shows the aircraft's altitude over the duration of the flight and the bottom graph shows the principle strains at one of the patches. The principle strains were calculated using standard delta rosette techniques. The direction of the first principle strain is along the length of the wing.

The altitude plot clearly indicates when the take-off, roller landings and the final full stop landing happened. Comparison of the strain and altitude graphs shows that there are significant strain changes at these take-off and landing points as would be expected.

## CONCLUSIONS

The technological evolution of the integrated optical AOTF offer a wide range of mature solutions for applications in the OFC systems, microwave signal processing and FBG sensor instrumentation fields. Significant efforts have been provided to improve the resolution of the AOTF avoiding the sidelobe ratio degradation caused by fabrication process disuniformities. The AOTF device has been used to realise rugged, portable, and high performance instrumentation for interrogation of FBG sensors to monitor both static and dynamic strains.

## REFERENCES

- [1] G.Meltz, W.W.Morey and W.H.Glenn, *Formation of Bragg gratings in optical fibers by a transverse holographic method*, Optics Letters, **14**, 823 (1989).
- [2] M Varasi, M Signorazzi, A Vannucci and Jim Dunphy, *A high-resolution integrated optical spectrometer with applications to fibre sensor signal processing*, Measurement Science and Technology, **7**,173 (1996).
- [3] J.Dunphy, G.Ball, F. D'Amato, P.Ferraro, S.Inserra, A.Vannucci, M.Varasi, *Distributed and multiplexed fiber optic sensors III*, Proceedings of the SPIE, **2071**, 2 (1993).
- [4] R.V. Schmidt, L.A. Coldren, *Thin film acoustic surface waveguides on anisotropic media*, IEEE Trans. on Sonics and Ultrasonics, **SU 22**, 115 (1975).
- [5] D.A.Smith et al., *Source of sidelobe asymmetry in integrated acousto-optic filters*, Applied Physics Letters, **62**, 814 (1993).